

Modern Hopfield Networks for Few- and Zero-Shot Reaction Template Prediction

Philipp Seidl* Philipp Renz*

Natalia Dyubankova[‡] Paulo Neves[‡] Jonaes Verhoeven[‡] Marwin Segler[§] Jörg K. Wegner[‡]

Sepp Hochreiter^{*,†} Günter Klambauer^{*}

*ELLIS Unit Linz, LIT AI Lab, Institute for Machine Learning,
Johannes Kepler University Linz, Austria

[†]Institute of Advanced Research in Artificial Intelligence (IARAI)

[‡]High Dimensional Biology and Discovery Data Sciences
Janssen Research & Development, Janssen Pharmaceutica N.V.

[§]Microsoft Research

Abstract

Finding synthesis routes for molecules of interest is an essential step in the discovery of new drugs and materials. To find such routes, computer-assisted synthesis planning (CASP) methods are employed, which rely on a model of chemical reactivity. In this study, we model single-step retrosynthesis in a template-based approach using modern Hopfield networks (MHNs). We adapt MHNs to associate different modalities, reaction templates and molecules, which allows the model to leverage structural information about reaction templates. This approach significantly improves the performance of template relevance prediction, especially for templates with few or zero training examples. With inference speed several times faster than baseline methods, we improve predictive performance for top-k exact match accuracy for $k \geq 5$ in the retrosynthesis benchmark USPTO-50k. Code to reproduce the results will be available at github.com/ml-jku/mhn-react.

1 Introduction

The design of a new molecule starts with an initial idea of a chemical structure with hypothesized desired properties [1]. Desired properties might be the inhibition of a disease or a virus in drug discovery or thermal stability in material science [2, 3]. From the design idea of the molecule, a virtual molecule is constructed, the properties of which can then be predicted by means of computational methods [4, 5]. However, to test its properties and to finally make use of it, the molecule has to be made physically available through chemical synthesis. Finding a synthesis route for a given molecule is a multi-step process that is considered highly complex [6].

To aid in finding synthesis routes, chemists have resorted to computer-assisted synthesis planning

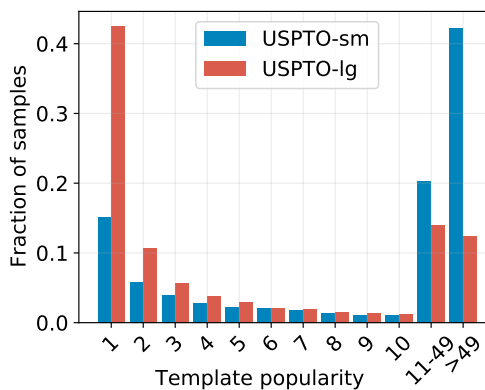


Figure 1: Histogram showing the fraction of samples for different template frequencies. The left-most red bar indicates that over 40% of chemical reactions of USPTO-lg have a unique reaction template. The majority of reaction templates are rare.

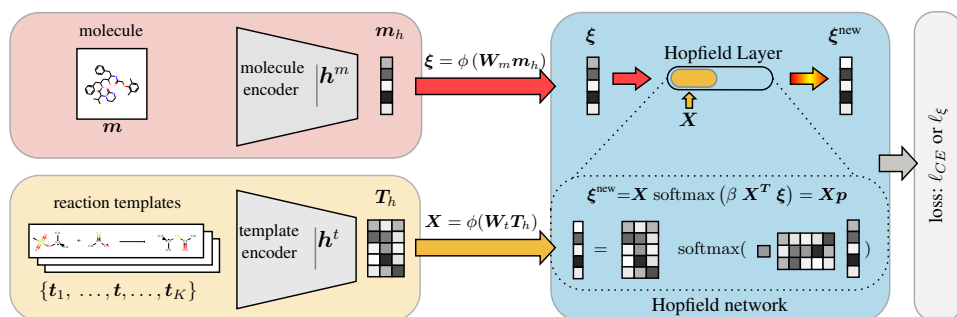


Figure 2: Simplified depiction of our approach. Standard approaches only encode the molecule and predict a fixed set of templates. In our MHN-based approach, the templates are also encoded and transformed to stored patterns via the template encoder. The Hopfield layer learns to associate the encoded input molecule, the state pattern ξ , with the memory of encoded templates, the stored patterns X . Multiple Hopfield layers can operate in parallel or be stacked using different encoders.

(CASP) methods [6, 7]. Chemical synthesis planning is often viewed in the retrosynthesis setting in which a molecule of interest is recursively decomposed into less complex molecules until only readily available precursor molecules remain [8]. Such an approach relies on a single-step retrosynthesis model, which, given a product, tries to propose sets of reactants from which it can be synthesized. Early methods modelled chemical reactivity using rule-based expert systems [7]. These methods, however, require extensive manual curation [8–10]. Recently there have been increased efforts to model chemical reactivity from reaction databases using machine learning methods [8, 11–13].

These efforts to model chemical reactions encompass a variety of different approaches. In one line of methods [13–18], the SMILES representation [19] of the reactants given that of the product is predicted, using architectures proposed initially for the translation between natural languages [20, 21]. Others exploit the graph structure of molecules and model the task using graph neural networks [22, 23]. A prominent line of work makes use of *reaction templates* which are graph transformation rules that encode connectivity changes between atoms during a chemical reaction.

In a template-based approach, reaction templates are first extracted from a reaction database or hand-coded by a chemist. If the product side of a template is a sub-graph of a molecule, the template is called applicable to the molecule, and can be used to transform it into a reactant set. However, even if a template can be applied to a molecule, the resulting reaction might not be viable in the lab [10]. Hence a core task, which we refer to as template-relevance prediction, in such an approach is to predict with which templates a molecule can be combined with to yield a viable reaction. In prior work, this problem has often been tackled using a machine learning methods that are trained at this task on a set of recorded reactions [8, 10, 24–30].

Template-based methods usually view the problem as a classification task in which the templates are modelled as distinct categories. However, this can be problematic as automatic template extraction leads to many templates that are represented by few training samples [8, 24]. Somnath et al. [23] argue that template-based approaches suffer from bad performance, particularly for rare reaction templates. Struble et al. [9] note that ML has not been applied successfully for CASP in low-data regimes. To address the low-data issue, Fortunato et al. [24] pretrained their template-relevance model to predict which templates are applicable and then fine-tuned it on recorded reactions in a database. This improved template-relevance prediction, especially for rare templates, as well as the average applicability of the top-ranked templates. Overall, a challenge of template-based methods arises from modelling reaction templates as distinct categories, which leads to many classes with few examples (see also Section 3).

To avoid the above-mentioned problems, we propose a new model that does not consider templates as distinct categories, but can leverage structural information about the template. This allows for generalization over templates and improves performance in the tasks defined in [24], especially for templates with few training samples and even for unseen templates. This model learns to associate relevant templates to product molecules using a Modern Hopfield Network [31, 32]. To this end, we

adapted MHNs to associate objects of different modalities, namely input molecules, and reaction templates. In contrast to popular ML approaches, in which variable or input-dependent subsets of the data are associated [20, 31, 33, 34], our architecture maintains a fixed set of representations, considered as a static memory independent of the input.

In this study, we propose a template-based method, which are often reported to be computationally expensive because of the NP-complete subgraph-isomorphism calculations involved in template execution [22–24, 26]. To address this issue Fortunato et al. [24] and Bjerrum et al. [26] trained neural networks to predict which templates are applicable given a molecule to filter inapplicable templates during inference. We find that using a substructure screen, i.e. a fast check of a necessary condition for a graph to be a subgraph of another, improves inference speed which may also be of interest for other template-based methods.

Contributions. In Section 3 we adapt modern Hopfield networks to associate different data modalities and to use a static memory resulting in a novel template-based approach to chemical synthesis. In Section 4 we demonstrate that our architecture improves predictive performance for template relevance prediction and single-step retrosynthesis. In Section 4.2 we investigate inference speed and show that our method is several times faster than baseline methods.

2 Background: single-step retrosynthesis

The goal of *single-step retrosynthesis* is to predict sets of molecules that react to a given product. As a molecule can be synthesized in various ways, this represents a one-to-many task. A model is thus expected to output a list of reactant sets sorted by a belief that a solution is correct. Performance in this setting is usually measured by *reactant top-k accuracy* using a reaction database. This metric measures the fraction of samples for which, given the product of a recorded reaction, the recorded reactants are among the top-k predictions. Given the one-to-many setting small values of k might not be an optimal choice as there might exist scenarios where a good model receives low scores. Choosing k too large might result in a metric that is too easy to optimize.

Template-based approaches predict reactant sets via reaction templates. A reaction template encodes atom connectivity changes during a chemical reaction and can be used to transform a product molecule to reactants, $m \xrightarrow{t} r$, where m is a product molecule, r represents a set of reactants and t a reaction template. The product side of a template encodes at which position in a molecule the template can be applied. A necessary condition for this is that the product side of the template is a substructure of the molecule of interest. If this is the case a template is said to be *applicable* to the molecule. The product sub-graph is then transformed according to the reactant side of the template and an atom-mapping between the two sides. Templates can be either hand-coded or automatically extracted from reaction databases, which yields an ordered set of K unique templates $\mathbf{T} = \{t^k\}_{k=1}^K$.

The aim of *template-relevance prediction* is to predict which templates result in a feasible reaction given a product. If this is the case we say that a template is *relevant* to a molecule. While applicability is a necessary condition for relevance, it ignores the context of the whole molecule and thus substructures that might conflict with the encoded reaction [10, Fig. 1]. In practice applicability gives poor performance at relevance prediction (see Table 1). To evaluate template-relevance predictions we use *template top-k accuracy*, which given the product of a recorded reaction measures the fraction of samples for which the template extracted from the recorded reaction is among the top-k predicted ones.

Given relevance predictions for a product, reactant sets are obtained by executing top-scoring templates. We do not permit relevance prediction to rely on applicability calculations because it is relatively slow to compute. Via this constraint, template top-k accuracy also incorporates information about the model’s ability to filter out non-applicable templates. This information might be lost in reactant accuracy as template execution relies on a check for applicability. Other differences between the reactant/template accuracy can arise from multiple locations in which the correct template may be applied or incorrect templates leading to the correct reactants.

3 Modern Hopfield networks for reaction template prediction

Motivation of our approach. Many template-based methods [8, 10, 24–26] predict templates using

$$\hat{\mathbf{y}} = \text{softmax}(\mathbf{W} \mathbf{h}^m(\mathbf{m})), \quad (1)$$

where $\mathbf{h}^m(\mathbf{m})$ is a neural network that maps a molecule representation to a vector of size d_m , which we call *molecule encoder*. Multiplication with $\mathbf{W} \in \mathbb{R}^{K \times d_m}$ yields a score for each template $\mathbf{t}_1, \dots, \mathbf{t}_K$. These scores are then normalized using the softmax function, which yields the vector $\hat{\mathbf{y}} \in \mathbb{R}^K$. In this setting, different templates are viewed as distinct categories or classes, which makes the model ignorant of similarities between classes which prevents generalization over templates. The high fraction of samples in reaction data sets that have a unique template can be problematic because they cannot contribute to performance. This problem might also appear for templates occurring only a few times, but to a lesser extent.

Instead of learning the rows of \mathbf{W} independently, one could map each template to a vector of size d_t using a *template encoder*, \mathbf{h}^t , and concatenate them row-wise to obtain $\mathbf{T}_h = \mathbf{h}^t(\mathbf{T}) \in \mathbb{R}^{K \times d_t}$. If $d_m = d_t$, replacing \mathbf{W} in the equation above yields

$$\hat{\mathbf{y}} = \text{softmax}(\mathbf{T}_h \mathbf{h}^m(\mathbf{m})), \quad (2)$$

which associates the molecule \mathbf{m} with each template via the dot product of their representations. This allows generalization across templates because the structure of the template is used to represent the class and the model can leverage similarities between templates. We adapt modern Hopfield networks [31, 35] to generalize this association of the two modalities, molecules and reaction templates.

A component of the model proposed in Dai et al. [27] is similar to our approach as it also makes use of the templates’ structures. Our approach also resembles the approach taken in CLIP [34] and ConVIRT [36] in which associated pairs of images and texts are contrasted against non-associated pairs. Our adaption of MHNs to maintain a static memory complements previous contrastive learning [33, 37] approaches using a memory [38–41].

Modern Hopfield networks. Recently Ramsauer et al. [31, 35] introduced modern Hopfield Networks (MHN) which are well-suited for learning associations between sets [32]. We use an MHN approach to generalize Eq. (2) to a more expressive association mapping

$$\hat{\mathbf{y}} = g(\mathbf{h}^m(\mathbf{m}), \mathbf{h}^t(\mathbf{T})), \quad (3)$$

where g consists of Hopfield layers based on MHNs. An MHN is an associative memory that stores patterns $\mathbf{X} \in \mathbb{R}^{d \times K}$ ¹ and iteratively updates a state pattern according to:

$$\boldsymbol{\xi}^{\text{new}} = \mathbf{X} \mathbf{p} = \mathbf{X} \text{softmax}(\beta \mathbf{X}^T \boldsymbol{\xi}), \quad (4)$$

where \mathbf{p} is called the vector of *associations* and $\beta > 0$ is a scaling parameter (inverse temperature). The update rule converges globally to stationary points of the energy function, $E = -\text{lse}(\beta, \mathbf{X}^T \boldsymbol{\xi}) + \frac{1}{2} \boldsymbol{\xi}^T \boldsymbol{\xi} + C$, where lse is the log-sum-exponential function, and C is a constant [31, Theorem 1 and 2]. To adapt MHNs to reaction template prediction, the Hopfield layer learns both a molecule representation used for the state pattern $\boldsymbol{\xi} \in \mathbb{R}^d$ and reaction template representations used for the stored patterns \mathbf{X} .

Model architecture with parallel or stacked Hopfield layers. Our model architecture consists of three main parts: a) a molecule encoder, b) a reaction template encoder, and c) one or more stacked or parallel Hopfield layers. Firstly, we use a molecule encoder function that learns a relevant representation for the task at hand. For this we use a fingerprint-based, e.g. ECFP [42], fully-connected NN, $\mathbf{h}_w^m(\mathbf{m})$ with weights w . The molecule encoder maps a molecule to its representation $\mathbf{m}_h = \mathbf{h}_w^m(\mathbf{m})$ of dimension d_m .

Secondly, we use the reaction template encoder \mathbf{h}_v^t with parameters v to learn relevant representations of templates. Here, we also use a fully-connected NN with *template fingerprints* as input. These fingerprints are described in Appendix Section A3. This function is applied to all templates \mathbf{T} and the resulting vectors are concatenated column-wise into a matrix $\mathbf{T}_h = \mathbf{h}_v^t(\mathbf{T})$ with shape (d_t, K) .

Finally, we use a single or several stacked or parallel Hopfield layers $g(\cdot, \cdot)$ to associate a molecule with all templates in the memory. The Hopfield layer consists of fully-connected layers with adaptive

¹Note that K in this work corresponds to N in [31].

weight matrices $\mathbf{W}_m, \mathbf{W}_t$ to map both molecule representations and template representations to a d -dimensional space: $\boldsymbol{\xi} = \phi(\mathbf{W}_m \mathbf{h}_w^m(\mathbf{m}))$ and $\mathbf{X} = \phi(\mathbf{W}_t \mathbf{h}_w^t(\mathbf{T}))$, where \mathbf{W}_m and \mathbf{W}_t are adaptive weight matrices with d rows, and ϕ is an activation function. Hopfield layers comprise layer normalization [43] for $\boldsymbol{\xi}$ and \mathbf{X} which is included as a hyperparameter. We also consider the scaling parameter β as a hyperparameter. The Hopfield layer then employs the update rule Eq. (4) through which the updated representation of the product molecule $\boldsymbol{\xi}^{\text{new}}$ and the vector of associations \mathbf{p} is obtained. If multiple Hopfield layers are stacked, $\boldsymbol{\xi}^{\text{new}}$ enters the next Hopfield layer, for which additional template encoders supply the template representations. Parallel Hopfield layers use the same template encoder, but learn different projections $\mathbf{W}_t, \mathbf{W}_m$, which is analogous to the heads in Transformer networks.

The simple model (Eq. 2) is a special case of our MHN and recovered if (a) \mathbf{W}_t and \mathbf{W}_m are the identity matrices and $d_t = d_m = d$, (b) the Hopfield network is constrained to a single update, (c) Hopfield networks are not stacked, i.e. there is only a single Hopfield layer (d) the scaling parameter $\beta = 1$, (e) layernorm learns zero mean and unit variance and does not use its adaptive parameters, and (f) the activation function ϕ is the identity. The standard DNN model (Eq. 1) is recovered if additionally the reaction templates are one-hot encoded, and the template encoder is linear.

In this study, we tested fingerprint-based fully-connected networks for the molecule and template encoder. In principle, one could use any mapping from molecules/templates to vector-valued representations for these components, for example raw fingerprints, graph neural networks [44] or SMILES/SMARTS-based RNNs [45] or Transformers [20].

Loss function and optimization. We provide a general definition of the loss in terms of retrieved patterns and details in Appendix Section A6. Here we supply a simple view of the case in which a single correct reaction template is assigned to each molecule. Given a training pair (\mathbf{m}, \mathbf{t}) and the set of all templates \mathbf{T} , the model should assign high probability to \mathbf{t} based on \mathbf{m} and \mathbf{T} . We encode this objective by the negative log-likelihood: $-\log p(\mathbf{t} | \mathbf{m}, \mathbf{T})$. The probability of each template in \mathbf{T} is encoded by the corresponding element of the vector of associations \mathbf{p} of the last Hopfield layer. In case of multiple parallel Hopfield layers, we use average pooling across the vectors \mathbf{p} supplied from each layer.

The parameters of the model are adjusted on a training set using stochastic gradient descent on the loss w.r.t. $\mathbf{W}_t, \mathbf{W}_m, \mathbf{w}, \mathbf{v}$ via the AdamW optimizer [46]. We train our model for a maximum of 100 epochs and then select the best model with respect to the minimum cross-entropy loss in the case of template-relevance prediction or maximum top-1 accuracy for single-step retrosynthesis on the validation set. Pseudo-code of the forward-pass of our model is presented in Alg. 1.

Regularization. We use dropout regularization in the molecule encoder \mathbf{h}^m , for the template encoder \mathbf{h}^t as well as for the representations in the Hopfield layers. We employ L2 regularization on the parameters. A detailed list of considered and selected hyperparameters is given in Appendix Tables A2 and A3.

Fingerprint filter (FPF). We added a computationally cheap fingerprint-based substructure screen as a post-processing step that can filter out a part of the non-applicable templates. For each product and the product side of each template, we calculated a bit-vector using the "PatternFingerprint" function from rdkit [47]. Each bit set in this vector specifies the presence of a substructure. For a template to be applicable every bit set in the template fingerprint also has to be set in the product fingerprint, which is a necessary condition for subgraphs to match. We chose a fingerprint size of 4096 as we did not observe significant performance gains for larger sizes, as can be seen in Appendix Fig. A2.

Algorithm 1 MHNs for template prediction (simplified)

```

# mol_encoder() Maps to dimension  $d_m$ .
# template_encoder() Maps to dimension  $d_t$ .
# m_train, t_train — pair of product molecule
and reaction template from training set
# T — set of  $K$  reaction templates including t_train
# d — dimension of Hopfield space
## forward pass
T_h = template_encoder(T)#[d_t,K]
m_h = mol_encoder(m_train)#[d_m,1]
xnew,p,X = Hopfield(m_h,T_h,dim=d)
p = pool(p,axis=1) #[K]
## association loss
label = where(T==t_train)#[K]
loss = cross_entropy(p,label)

```

4 Experiments

Data and preprocessing. All data sets used in this study are derived from the USPTO data set, extracted from the U.S. patent literature by Lowe [48]. This data set contains 1.8M text-mined reaction equations in SMILES notation [19] and consists of reactions recorded in the years from 1976 to 2016. Reaction conditions and process actions are not included. For evaluating template relevance prediction, we use the preprocessing procedure described in [24]. Templates are extracted using rdchiral [49]. This results in two data sets, *USPTO-sm* which is based on USPTO-50k [50] and *USPTO-lg* which is based on USPTO-410k [51]. For evaluating single-step retrosynthesis we use USPTO-50k as preprocessed in [29]. For this set we also extract templates using rdchiral [49], but only for the train- and validation split to prevent test data leakage. A detailed description of the data sets and their preprocessing can be found in Appendix A3.

Compute time and resources. All experiments were run on different servers with diverse Nvidia GPUs (Titan V 12GB, P40 24 GB, V100 16GB, A100 20GB MIG) using PyTorch 1.6.0 [52]. We estimate the total run-time to be around 1000 GPU hours. A single MHN model can be trained on USPTO-50k in approximately 5 minutes on a V100. **Metrics.** We measure performance for template-relevance prediction using template top-k accuracy, and use reactant top-k accuracy for evaluating single-step retrosynthesis as described in Section 2.

4.1 Template relevance prediction: USPTO-sm and USPTO-lg

In this section, we investigate template-relevance prediction models in detail. We first compare the performance of our method to previously suggested ones. Then we analyze how performance varies as a function of template frequency. Next we show that our method can make use of a larger fraction of the training data than a baseline method. We conclude the section with an ablation study showing the importance of different modelling parameters.

We analyze the differences between our MHN method and two related previously suggested ones: Firstly, a fully-connected network with a softmax output, **DNN**, in which each output unit corresponds to a reaction template similar to [10]. Secondly, **DNN+pretrain**, which is the same as the above but including a pretraining-step on template applicability [24]. The main differences between these and our MHN method are the choice of network architecture (DNN/MHN), whether the FPF is used and whether the pretraining step on applicability prediction is included. This results in eight possible method variants which we include in our studies. Additionally, we report the results for a naive baseline **Pop+FPF**, which ranks templates by their popularity in the training set and applies the FPF. For all methods hyperparameters were adjusted on the validation set as described in Appendix Section A3.

Comparison to previous methods. We compared the predictive performance of our MHN approach to two closely related previously suggested template-relevance prediction methods (DNN/DNN+Pretrain) and the popularity baseline (Pop) on the USPTO-sm/lg data sets described above. The grey rows in Table 1 show that for most of the investigated settings our method exhibits better performance than these related methods, sometimes by a large margin. Only for top-1 accuracy on USPTO-lg the DNN model with FPF or pre-training outperformed the MHN model.

Rare templates: few- and zero-shot learning. Next we investigated how the predictive performance for samples varies as a function of number of training samples with the same template. We again compared the methods introduced in the paragraph above. Figure 3 shows the top-100 accuracy for different subsets of the test set, which were grouped by the number of training samples with the same template. Especially for samples with rare templates the performance gap between our method and the compared ones is large. The DNN models and the popularity baseline perform very poorly for samples with templates not seen during training, which is expected as they cannot generalize across templates. The MHN model on the other hand achieves far above random accuracy on these samples. The performance on samples with rare templates has a considerable impact on overall performance due to the large number of templates that occur only few times in the training set.

Learning from rare templates. Next we analyze the effect on performance of rare template samples in the training set. In a classification setting, it is only useful to include classes if they are recurring, i.e. represented by more than one sample. However, in the USPTO-sm/lg datasets many templates occur only once (see Fig. 1). If the templates are modelled as categories as done in the DNN approach,

Table 1: Template top-k accuracy (%) of different method variants on USPTO-sm and USPTO-lg. "Model" indicates how the templates were ranked. "Filter" specifies if and how templates were excluded from the ranking via FPF or an applicability check (App). Pre-train indicates whether a model was pre-trained on the applicability task. Error bars represent confidence intervals on binomial proportions. The grey rows indicate methods specifically proposed here or in prior work.

Ref.	Model	Filter	Pretrain	USPTO-sm			USPTO-lg		
				Top-1	Top-10	Top-100	Top-1	Top-10	Top-100
[10]	DNN	-	no	38.1 ^a	64.1 ^a	76.5 ^a	16.0 ^b	35.7 ^b	50.7 ^b
[24]	DNN	-	yes	38.5 ^a	69.1 ^a	85.8 ^a	20.8 ^b	41.7 ^b	54.2 ^b
	DNN	FPF	no	39.0 ^a	67.6 ^a	84.6 ^a	17.1 ^b	38.1 ^b	53.6 ^b
	DNN	FPF	yes	38.9 ^a	71.2 ^a	90.6 ^a	21.5^b	43.0 ^b	56.0 ^b
	MHN	-	no	39.9 ^a	75.7 ^a	91.9 ^a	16.7 ^b	43.6 ^b	71.4 ^b
	MHN	-	yes	40.4^a	76.2^a	91.8^a	16.7 ^b	43.5 ^b	71.4 ^b
(ours)	MHN	FPF	no	40.5^a	78.7^a	95.9^a	16.9 ^b	44.2^b	72.4^b
	MHN	FPF	yes	41.3^a	78.8^a	95.7^a	17.0 ^b	44.1^b	72.3^b
	Pop	-	no	0.0 ^a	8.6 ^a	28.9 ^a	0.1 ^b	0.8 ^b	3.5 ^b
	Pop	FPF	no	1.5 ^a	17.6 ^a	53.1 ^a	0.3 ^b	1.9 ^b	7.5 ^b
	Pop	App ^c	no	9.4 ^a	39.6 ^a	80.3 ^a	1.1 ^b	5.1 ^b	16.5 ^b

^a width of 95%-confidence interval < 1.3 %.

^b width of 95%-confidence interval < 0.4 %.

^c note that the applicability filter violates the modelling constraints given in Section 2.

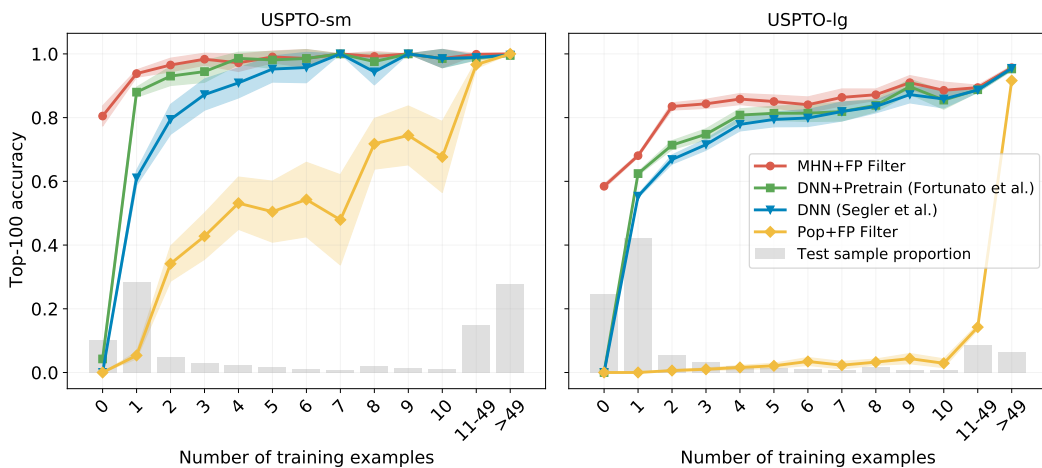


Figure 3: Top-100 accuracy for different template popularity on the USPTO-sm/lg datasets. The grey bars represent proportion of samples in the test set. Error bars represent 95%-confidence intervals on binomial proportion. Our method performs especially well on samples with reaction templates with few training examples.

Table 2: Reactant top-k accuracy (%) on USPTO-50k retrosynthesis. Bold values indicate values within 0.1, green 1 and yellow within 3 percentage points to the maximum value. Error bars represent standard deviations across five re-runs. Category ("Cat.") indicates whether a method is template-based (tb) or template-free (tf). Methods in the upper part have been (re-)implemented in this work.

Abbr.	Ref.	Cat.	Top-1	Top-3	Top-5	Top-10	Top-20	Top-50
MHNreact	ours	tb	50.5 \pm .3	73.9 \pm .3	81.0\pm.1	87.9\pm.2	92.0\pm.1	94.1\pm.0
Neuralsym	[10]	tb	45.2 \pm .2	67.9 \pm .5	75.8 \pm .2	83.5 \pm .2	89.1 \pm .1	93.5 \pm .1
Pop		tb	18.4	38.7	48.6	63.0	75.8	89.8
Dual-TB	[53]	tb	55.2	74.6	80.5	86.9		
Dual-TF	[53]	tf	53.3	69.7	73.0	75.0		
ATx100	[54]	tf	53.5		81.0	85.7		
GLN	[18]	tb	52.5	69.0	75.6	83.7	89.0	92.4
RetroPrime	[27]	tf	51.4	74.0	74.0	76.1		
G2G	[55]	tf	48.9	67.6	72.5	75.5		
MEGAN	[22]	tf	48.6	72.2	80.3	87.6	91.6	94.2
GET-LT1	[56]	tf	44.9	58.8	62.4	65.9		
Neuralsym	[10, 27]	tb	44.4	65.3	72.4	78.9	82.2	83.1
GOPRO	[57]	tf	43.8	57.2	61.4	66.6		
SCROP	[58]	tf	43.7	60.0	65.2	68.7		
LV-Trans	[59]	tf	40.5	65.1	72.8	79.4		
Trans	[17]	tf	37.9	57.3	62.7			
Retrosim	[29]	tb	37.3	54.7	63.3	74.1	82.0	85.3

a large fraction of samples cannot contribute to performance. However, this does not hold for models that can generalize across templates, as our MHN model is able to do. To show the effect of the rare template samples on learning, we use the following experiment on USPTO-sm: We removed all samples with templates that are *exactly once* in the training set and *not* in the test set and retrain the best DNN and MHN models of the template relevance prediction experiment. After removal of these samples, the top-10 accuracy rose from 71.1 \pm .2 to 72.3 \pm .2 for the DNN+pretrain model and dropped from 78.8 \pm .4 to 73.7 \pm .3 for the MHN model. As expected, the performance does not drop for the DNN model, but even improved marginally, which we attribute to the model knowing which templates do not occur in the test set. In contrast, the performance for the MHN model decreased. This shows that the increased performance of our approach is in part caused by the larger fraction of data that can be leveraged for learning.

Ablation study. Next, we investigated the importance of the main parameters of the methods reported in this section, concretely the choice of network architecture (DNN/MHN), whether the FPF is used, and whether pre-training on applicability is performed. We evaluated the eight possible parameter variations on USPTO-sm/lg. The upper section of Table 1 shows the predictive performance of these methods. We observe that the columns are approximately sorted from top-to-bottom. In combination with the organization of the method columns, this implies that MHN contributes the most to improved performance, followed by FPF and the use of pre-training. The lower part of Table 1 shows the performance of the popularity baseline. The last row shows that a plain applicability check is not sufficient for high performance. We include additional results in Appendix Section A3.

4.2 Single-step retrosynthesis: USPTO-50k

Next we compare our method to previously suggested ones in the single-step retrosynthesis task using the USPTO-50k data set. We follow the preprocessing procedure of [12] and used rdchiral [49] to extract reaction templates. Following [12] we shuffled the data and assign 80/10/10% of the samples in each reaction class into train/validation/test set respectively. This is similar to USPTO-sm above but varies in details discussed in Appendix Section A3. We first compare the predictive performance of our method to previous ones and then investigate its inference speed.

Predictive performance. Table 2 shows the reactant top-k accuracies for different methods. These methods include, among others, transformer-based [18, 54], graph-to-graph [55] or template-based

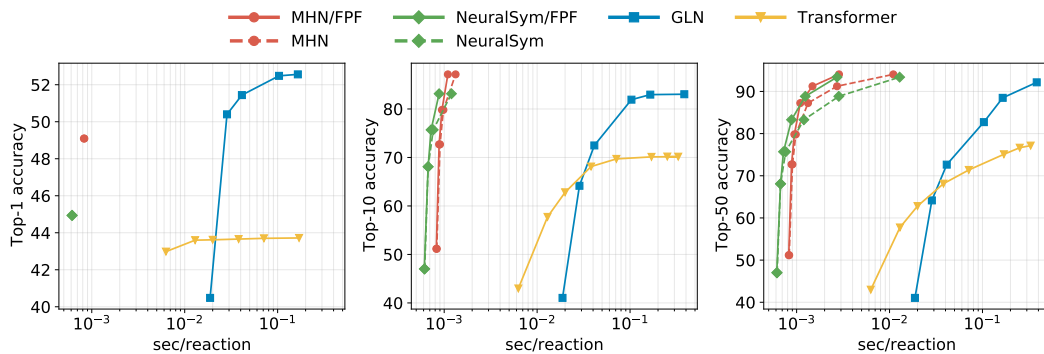


Figure 4: Reactant top-k accuracy vs. inference speed for different values of k. Upper left is better. For Transformer/GLN the points represent different beam sizes. For MHN/NeuralSym the points reflect different numbers of generated reactant sets, namely $\{1, 3, 5, 10, 20, 50\}$.

ones [27]. Some methods [16, 23, 60–65] that also report results on USPTO-50k were omitted here, either due to test set leakage or a different evaluation conditions, as detailed Appendix Section A3. We re-implemented and improved the NeuralSym method as described in Appendix Section A3. and added the popularity baseline described in Section 4.1. Hyperparameter selection on the validation set returned an MHN model with two stacked Hopfield layers, which we refer to as *MHNreact* (see Appendix Section A3). We ranked reactant sets by the score of the template used to produce them. If a template execution yielded multiple results all were included in the prediction in random order. Table 2 shows reactant top-k accuracy for different methods. Our method achieved state-of-the-art performance for $k \geq 5$ and approaches it for $k = 1, 3$. Together with Dual-TB [53] this puts template-based methods ahead of other approaches at all considered values of k.

Inference speed. Aside from predictive performance, inference speed is also vital for retrosynthesis methods. Therefore, CASP methods are often evaluated by their ability to find a route in a given time [8, 26, 66]. Template-based methods are sometimes reported to be slow [22, 54], however we found that inference speed was not reported in mentioned studies and are seldom reported in general, despite their importance. Accuracy can be traded for inference speed for many models. For some, this trade-off is achieved by varying beam size [18, 27]. In template-based approaches, the number of executed templates can be varied and traded off against speed. We compared inference speed of our MHN method with the following baselines. We obtained results for GLN from their paper [22]. We trained a Transformer baseline using the code of [13], as a representative of transformer-based methods [17, 18, 59]. Additionally, we also include the NeuralSym [10] model we implemented in the comparison. The results are displayed in Fig. 4. At comparable or better performance, our method achieves inference speed of up to two magnitudes faster compared to Transformer and GLN. While NeuralSym is faster than our model for some fixed values of accuracy, MHN yields better maximum accuracy with comparable speed.

5 Discussion and conclusion

We have introduced a new Deep Learning architecture for reaction template prediction based on modern Hopfield networks. To this end, we have adapted modern Hopfield networks to associate objects of different modalities and to use a static memory. This type of multi-modal learning might be relevant in other areas, in which two or more data modalities have to be associated based on limited available data. The architecture comprises a molecule and reaction template encoder networks. The latter enables generalization across templates which enables zero-shot learning and improves few-shot learning. On the single-step retrosynthesis benchmark USPTO-50k, our model MHNreact reaches state-of-the-art at top-k accuracy for $k \geq 5$. We found little data that back the common claim of template-based methods being slow and hope that we contributed data that shed a new light on this matter. We envision that our approach will be used to improve CASP systems or synthesis-aware generative models [67–70].

Limitations. Our experiments are currently limited by several factors. We did not investigate the importance of radius around the reaction center used for template extraction. We currently do not re-rank reactants based on a secondary model such as an in-scope filter [8] or dual models [53], which could increase performance. The scalability of our method remains to be investigated. The results for inference speed depend highly on implementation and may potentially be improved by relatively simple means.

Potential biases, consequences of failure and societal impact. Since the inputs to our model do not contain data of individuals, there are no direct biases or unfairness towards a particular gender, age or ethnic groups. However, there are still biases towards particular chemical spaces or reactions that have been introduced by humans. Our approach can help to speed up the discovery of molecules or to find new, and more efficient synthesis routes. While new molecules can serve as medicines, secure the world's food supply via agrochemicals, or enable a sustainable energy conversion and storage to counter or mitigate climate change, such new molecules might also be toxins or pollutants, which negatively impact humanity. As common with methods in machine learning, potential danger lies in the possibility that users rely too much on our new approach and use it without reflecting on the outcomes. However, the full pipeline in which our method would be used includes wet lab tests after its application to verify and investigate the results, gain insights, and possibly derive treatments. Failures of the proposed method would lead to adverse outcomes in wet lab tests.

Acknowledgements

The ELLIS Unit Linz, the LIT AI Lab, the Institute for Machine Learning, are supported by the Federal State Upper Austria. IARAI is supported by Here Technologies. We thank the projects AI-MOTION (LIT-2018-6-YOU-212), AI-SNN (LIT-2018-6-YOU-214), DeepFlood (LIT-2019-8-YOU-213), Medical Cognitive Computing Center (MC3), PRIMAL (FFG-873979), S3AI (FFG-872172), DL for granular flow (FFG-871302), ELISE (H2020-ICT-2019-3 ID: 951847), AIDD (MSCA-ITN-2020 ID: 956832). We thank Janssen Pharmaceutica (MaDeSMart, HBC.2018.2287), Audi.JKU Deep Learning Center, TGW LOGISTICS GROUP GMBH, Silicon Austria Labs (SAL), FILL Gesellschaft mbH, Anyline GmbH, Google, ZF Friedrichshafen AG, Robert Bosch GmbH, UCB Biopharma SRL, Merck Healthcare KGaA, Software Competence Center Hagenberg GmbH, TÜV Austria, and the NVIDIA Corporation.

References

- [1] Joseph G. Lombardino and John A. Lowe. "The Role of the Medicinal Chemist in Drug Discovery — Then and Now". In: *Nature Reviews Drug Discovery* 3.10 (2004), pp. 853–862. URL: <https://doi.org/10.1038/nrd1523>.
- [2] Zhichao Lu et al. "Interpretable machine-learning strategy for soft-magnetic property and thermal stability in Fe-based metallic glasses". In: *npj Computational Materials* 6.1 (2020), pp. 1–9. URL: <https://www.nature.com/articles/s41524-020-00460-x>.
- [3] Andreas Mayr, Günter Klambauer, Thomas Unterthiner, Marvin Steijaert, Jörg K Wegner, Hugo Ceulemans, Djork-Arné Clevert, and Sepp Hochreiter. "Large-scale comparison of machine learning methods for drug target prediction on ChEMBL". In: *Chemical science* 9.24 (2018), pp. 5441–5451. URL: <https://pubs.rsc.org/en/content/articlelanding/2018/SC/C8SC00148K>.
- [4] J. A. McCammon. "Computer-Aided Molecular Design". In: *Science* 238.4826 (1987), pp. 486–491. URL: <https://doi.org/10.1126/science.3310236>.
- [5] Lik Yin Ng, Fah Keen Chong, and Nishanth G. Chemmangattuvalappil. "Challenges and Opportunities in Computer-Aided Molecular Design". In: *Computers & Chemical Engineering* 81 (2015), pp. 115–129. URL: <https://doi.org/10.1016/j.compchemeng.2015.03.009>.
- [6] E. J. Corey and W. Todd Wipke. "Computer-Assisted Design of Complex Organic Syntheses". In: *Science* 166.3902 (1969), pp. 178–192.
- [7] Sara Szymkuć, Ewa P. Gajewska, Tomasz Klucznik, Karol Molga, Piotr Dittwald, Michał Startek, Michał Bajczyk, and Bartosz A. Grzybowski. "Computer-Assisted Synthetic Planning: The End of the Beginning". In: *Angewandte Chemie International Edition* 55.20 (2016), pp. 5904–5937. URL: <https://doi.org/10.1002/anie.201506101>.

- [8] Marwin H. S. Segler, Mike Preuss, and Mark P. Waller. “Planning Chemical Syntheses with Deep Neural Networks and Symbolic AI”. In: *Nature* 555.7698 (2018), pp. 604–610. URL: <https://doi.org/10.1038/nature25978>.
- [9] Thomas J. Struble et al. “Current and Future Roles of Artificial Intelligence in Medicinal Chemistry Synthesis”. In: *Journal of Medicinal Chemistry* 63.16 (2020), pp. 8667–8682. URL: <https://doi.org/10.1021/acs.jmedchem.9b02120>.
- [10] Marwin H. S. Segler and Mark P. Waller. “Neural-Symbolic Machine Learning for Retrosynthesis and Reaction Prediction”. In: *Chemistry* 23.25 (2017), pp. 5966–5971. URL: <https://doi.org/10.1002/chem.201605499>.
- [11] Connor W. Coley, William H. Green, and Klavs F. Jensen. “Machine Learning in Computer-Aided Synthesis Planning”. In: *Accounts of Chemical Research* 51.5 (2018), pp. 1281–1289. URL: <https://doi.org/10.1021/acs.accounts.8b00087>.
- [12] Connor W. Coley, Luke Rogers, William H. Green, and Klavs F. Jensen. “Computer-Assisted Retrosynthesis Based on Molecular Similarity”. In: *ACS Central Science* 3.12 (2017), pp. 1237–1245. URL: <https://doi.org/10.1021/acscentsci.7b00355>.
- [13] Philippe Schwaller, Teodoro Laino, Théophile Gaudin, Peter Bolgar, Christopher A. Hunter, Costas Bekas, and Alpha A. Lee. “Molecular Transformer: A Model for Uncertainty-Calibrated Chemical Reaction Prediction”. In: *ACS Central Science* 5.9 (2019), pp. 1572–1583. URL: <https://doi.org/10.1021/acscentsci.9b00576>.
- [14] Juno Nam and Jurae Kim. *Linking the Neural Machine Translation and the Prediction of Organic Chemistry Reactions*. 2016. arXiv: 1612.09529. URL: <http://arxiv.org/abs/1612.09529>.
- [15] Philippe Schwaller, Théophile Gaudin, Dávid Lányi, Costas Bekas, and Teodoro Laino. ““Found in Translation”: Predicting Outcomes of Complex Organic Chemistry Reactions Using Neural Sequence-to-Sequence Models”. In: *Chemical Science* 9.28 (2018), pp. 6091–6098. URL: <https://doi.org/10.1039/C8SC02339E>.
- [16] Bowen Liu et al. “Retrosynthetic Reaction Prediction Using Neural Sequence-to-Sequence Models”. In: *ACS Central Science* 3.10 (2017), pp. 1103–1113. URL: <https://doi.org/10.1021/acscentsci.7b00303>.
- [17] Pavel Karpov, Guillaume Godin, and Igor V. Tetko. “A Transformer Model for Retrosynthesis”. In: Springer International Publishing, 2019, pp. 817–830.
- [18] Igor V. Tetko, Pavel Karpov, Ruud Van Deursen, and Guillaume Godin. “State-of-the-Art Augmented NLP Transformer Models for Direct and Single-Step Retrosynthesis”. In: *Nature Communications* 11.1 (2020), p. 5575. URL: <https://doi.org/10.1038/s41467-020-19266-y>.
- [19] David Weininger. “SMILES, a Chemical Language and Information System”. In: *Journal of Chemical Information and Computer Sciences* 28.1 (1988), pp. 31–36. URL: <https://doi.org/10.1021/ci00057a005>.
- [20] Ashish Vaswani, Noam Shazeer, Niki Parmar, Jakob Uszkoreit, Llion Jones, Aidan N. Gomez, Lukasz Kaiser, and Illia Polosukhin. *Attention Is All You Need*. 2017. arXiv: 1706.03762. URL: <http://arxiv.org/abs/1706.03762>.
- [21] Ilya Sutskever, Oriol Vinyals, and Quoc V Le. “Sequence to sequence learning with neural networks”. In: *Proceedings of the 27th International Conference on Neural Information Processing Systems-Volume 2*. 2014, pp. 3104–3112.
- [22] Chence Shi, Minkai Xu, Hongyu Guo, Ming Zhang, and Jian Tang. *A Graph to Graphs Framework for Retrosynthesis Prediction*. 2020. arXiv: 2003.12725.
- [23] Vignesh Ram Somnath, Charlotte Bunne, Connor W. Coley, Andreas Krause, and Regina Barzilay. *Learning Graph Models for Template-Free Retrosynthesis*. 2020. arXiv: 2006.07038. URL: <http://arxiv.org/abs/2006.07038>.
- [24] Michael E. Fortunato, Connor W. Coley, Brian C. Barnes, and Klavs F. Jensen. “Data Augmentation and Pretraining for Template-Based Retrosynthetic Prediction in Computer-Aided Synthesis Planning”. In: *Journal of Chemical Information and Modeling* 60.7 (2020), pp. 3398–3407. URL: <https://doi.org/10.1021/acs.jcim.0c00403>.
- [25] Jennifer N. Wei, David Duvenaud, and Alán Aspuru-Guzik. “Neural Networks for the Prediction of Organic Chemistry Reactions”. In: *ACS Central Science* 2.10 (2016), pp. 725–732. URL: <https://doi.org/10.1021/acscentsci.6b00219>.

- [26] Esben Jannik Bjerrum, Amol Thakkar, and Ola Engkvist. "Artificial Applicability Labels for Improving Policies in Retrosynthesis Prediction". In: *Machine Learning: Science and Technology* 2.1 (2020), p. 017001. URL: <https://doi.org/10.1088/2632-2153/abcf90>.
- [27] Hanjun Dai, Chengtao Li, Connor W. Coley, Bo Dai, and Le Song. *Retrosynthesis Prediction with Conditional Graph Logic Network*. 2020. arXiv: 2001.01408. URL: <http://arxiv.org/abs/2001.01408>.
- [28] Javier L. Baylon, Nicholas A. Cilfone, Jeffrey R. Gulcher, and Thomas W. Chittenden. "Enhancing Retrosynthetic Reaction Prediction with Deep Learning Using Multiscale Reaction Classification". In: *Journal of Chemical Information and Modeling* 2 (2019). URL: <https://doi.org/10.1021/acs.jcim.8b00801>.
- [29] Connor W. Coley, Luke Rogers, William H. Green, and Klavs F. Jensen. "Computer-Assisted Retrosynthesis Based on Molecular Similarity". In: *ACS Central Science* 3.12 (2017), pp. 1237–1245. URL: <https://pubs.acs.org/doi/10.1021/acscentsci.7b00355>.
- [30] Shoichi Ishida, Kei Terayama, Ryosuke Kojima, Kiyosei Takasu, and Yasushi Okuno. "Prediction and Interpretable Visualization of Retrosynthetic Reactions Using Graph Convolutional Networks". In: *Journal of Chemical Information and Modeling* 59.12 (2019), pp. 5026–5033. URL: <https://doi.org/10.1021/acs.jcim.9b00538>.
- [31] Hubert Ramsauer et al. *Hopfield Networks Is All You Need*. 2020. arXiv: 2008.02217. URL: <http://arxiv.org/abs/2008.02217>.
- [32] Michael Widrich et al. *Modern Hopfield Networks and Attention for Immune Repertoire Classification*. 2020. arXiv: 2007.13505. URL: <http://arxiv.org/abs/2007.13505>.
- [33] Ting Chen, Simon Kornblith, Mohammad Norouzi, and Geoffrey Hinton. "A Simple Framework for Contrastive Learning of Visual Representations". In: International Conference on Machine Learning. PMLR, 2020, pp. 1597–1607. URL: <http://proceedings.mlr.press/v119/chen20j.html>.
- [34] Alec Radford et al. *Learning Transferable Visual Models From Natural Language Supervision*. 2021. arXiv: 2103.00020.
- [35] Hubert Ramsauer et al. "Hopfield Networks is All You Need". In: *International Conference on Learning Representations*. 2021. URL: <https://openreview.net/forum?id=tL89RnzIiCd>.
- [36] Yuhao Zhang, Hang Jiang, Yasuhide Miura, Christopher D. Manning, and Curtis P. Langlotz. *Contrastive Learning of Medical Visual Representations from Paired Images and Text*. 2020. arXiv: 2010.00747. URL: <http://arxiv.org/abs/2010.00747>.
- [37] R. Hadsell, S. Chopra, and Y. LeCun. "Dimensionality Reduction by Learning an Invariant Mapping". In: 2006 IEEE Computer Society Conference on Computer Vision and Pattern Recognition (CVPR'06). Vol. 2. 2006, pp. 1735–1742. URL: <https://doi.org/10.1109/CVPR.2006.100>.
- [38] Z. Wu, Y. Xiong, S. X. Yu, and D. Lin. "Unsupervised Feature Learning via Non-parametric Instance Discrimination". In: *IEEE/CVF Conference on Computer Vision and Pattern Recognition (CVPR)*. 2018, pp. 3733–3742. DOI: 10.1109/CVPR.2018.00393.
- [39] Ishan Misra and Laurens van der Maaten. "Self-Supervised Learning of Pretext-Invariant Representations". In: Proceedings of the IEEE/CVF Conference on Computer Vision and Pattern Recognition. 2020, pp. 6707–6717. URL: https://openaccess.thecvf.com/content_CVPR_2020/html/Misra_Self-Supervised_Learning_of_Pretext-Invariant_Representations_CVPR_2020_paper.html.
- [40] Kaiming He, Haoqi Fan, Yuxin Wu, Saining Xie, and Ross Girshick. "Momentum Contrast for Unsupervised Visual Representation Learning". In: Proceedings of the IEEE/CVF Conference on Computer Vision and Pattern Recognition. 2020, pp. 9729–9738. URL: https://openaccess.thecvf.com/content_CVPR_2020/html/He_Momentum_Contrast_for_Unsupervised_Visual_Representation_Learning_CVPR_2020_paper.html.
- [41] Yonglong Tian, Dilip Krishnan, and Phillip Isola. *Contrastive Multiview Coding*. 2020. arXiv: 1906.05849. URL: <http://arxiv.org/abs/1906.05849>.
- [42] David Rogers and Mathew Hahn. "Extended-Connectivity Fingerprints". In: *Journal of Chemical Information and Modeling* 50.5 (2010), pp. 742–754. URL: <https://doi.org/10.1021/ci100050t>.
- [43] Jimmy Lei Ba, Jamie Ryan Kiros, and Geoffrey E. Hinton. *Layer Normalization*. 2016. arXiv: 1607.06450. URL: <http://arxiv.org/abs/1607.06450>.

- [44] Justin Gilmer, Samuel S. Schoenholz, Patrick F. Riley, Oriol Vinyals, and George E. Dahl. “Neural Message Passing for Quantum Chemistry”. In: International Conference on Machine Learning. PMLR, 2017, pp. 1263–1272. URL: <http://proceedings.mlr.press/v70/gilmer17a.html>.
- [45] Andreas Mayr, Günter Klambauer, Thomas Unterthiner, Marvin Steijaert, Jörg K. Wegner, Hugo Ceulemans, Djork-Arné Clevert, and Sepp Hochreiter. “Large-Scale Comparison of Machine Learning Methods for Drug Target Prediction on ChEMBL”. In: *Chemical Science* (2018). URL: <https://doi.org/10.1039/C8SC00148K>.
- [46] Ilya Loshchilov and Frank Hutter. “Fixing Weight Decay Regularization in Adam”. In: (2018). URL: <https://openreview.net/forum?id=rk6qdGgCZ>.
- [47] Greg Landrum. *RDKit: Open-Source Cheminformatics*. 2006. URL: <http://www.rdkit.org>.
- [48] Daniel Mark Lowe. “Extraction of Chemical Structures and Reactions from the Literature”. 2012. URL: <https://doi.org/10.17863/CAM.16293>.
- [49] Connor W. Coley, William H. Green, and Klavs F. Jensen. “RDChiral: An RDKit Wrapper for Handling Stereochemistry in Retrosynthetic Template Extraction and Application”. In: *Journal of Chemical Information and Modeling* 59.6 (2019), pp. 2529–2537. URL: <https://doi.org/10.1021/acs.jcim.9b00286>.
- [50] Nadine Schneider, Nikolaus Stiefl, and Gregory A. Landrum. “What’s What: The (Nearly) Definitive Guide to Reaction Role Assignment”. In: *Journal of Chemical Information and Modeling* 56.12 (2016), pp. 2336–2346. URL: <https://doi.org/10.1021/acs.jcim.6b00564>.
- [51] Connor W. Coley, Wengong Jin, Luke Rogers, Timothy F. Jamison, Tommi S. Jaakkola, William H. Green, Regina Barzilay, and Klavs F. Jensen. “A Graph-Convolutional Neural Network Model for the Prediction of Chemical Reactivity”. In: *Chemical Science* 10.2 (2019), pp. 370–377. URL: <https://doi.org/10.1039/C8SC04228D>.
- [52] Adam Paszke et al. *PyTorch: An Imperative Style, High-Performance Deep Learning Library*. 2019. arXiv: 1912.01703. URL: <http://arxiv.org/abs/1912.01703>.
- [53] Ruoxi Sun, Hanjun Dai, Li Li, Steven Kearnes, and Bo Dai. *Energy-Based View of Retrosynthesis*. 2020. arXiv: 2007.13437. URL: <https://openreview.net/forum?id=0Hj3tFCSjUd>.
- [54] Mikołaj Sacha, Mikołaj Błaż, Piotr Byrski, Paweł Włodarczyk-Pruszyński, and Stanisław Jastrzębski. *Molecule Edit Graph Attention Network: Modeling Chemical Reactions as Sequences of Graph Edits*. 2020. arXiv: 2006.15426. URL: <http://arxiv.org/abs/2006.15426>.
- [55] Xiaorui Wang, Yuquan Li, Jiezhong Qiu, Guangyong Chen, Huanxiang Liu, Benben Liao, Chang-Yu Hsieh, and Xiaojun Yao. “RetroPrime: A Diverse, Plausible and Transformer-Based Method for Single-Step Retrosynthesis Predictions”. In: *Chemical Engineering Journal* 420 (2021), p. 129845. URL: <https://doi.org/10.1016/j.cej.2021.129845>.
- [56] Kelong Mao, Peilin Zhao, Tingyang Xu, Yu Rong, Xi Xiao, and Junzhou Huang. “Molecular Graph Enhanced Transformer for Retrosynthesis Prediction”. In: *bioRxiv* (2020), p. 2020.03.05.979773. URL: <https://doi.org/10.1101/2020.03.05.979773>.
- [57] Vipul Mann and Venkat Venkatasubramanian. *Retrosynthesis Prediction Using Grammar-Based Neural Machine Translation: An Information-Theoretic Approach*. 2021. chemrxiv: 14410442.v1. URL: <https://doi.org/10.26434/chemrxiv.14410442.v1>.
- [58] Shuangjia Zheng, Jiahua Rao, Zhongyue Zhang, Jun Xu, and Yuedong Yang. “Predicting Retrosynthetic Reactions Using Self-Corrected Transformer Neural Networks”. In: *Journal of Chemical Information and Modeling* 60.1 (2020), pp. 47–55. URL: <https://doi.org/10.1021/acs.jcim.9b00949>.
- [59] Benson Chen, Tianxiao Shen, Tommi S. Jaakkola, and Regina Barzilay. *Learning to Make Generalizable and Diverse Predictions for Retrosynthesis*. 2019. arXiv: 1910.09688. URL: <http://arxiv.org/abs/1910.09688>.
- [60] Chaochao Yan, Qianggang Ding, Peilin Zhao, Shuangjia Zheng, Jinyu Yang, Yang Yu, and Junzhou Huang. *RetroXpert: Decompose Retrosynthesis Prediction like a Chemist*. 2020. arXiv: 2011.02893. URL: <http://arxiv.org/abs/2011.02893>.
- [61] Hankook Lee, Sungsoo Ahn, Seung-Woo Seo, You Young Song, Sung-Ju Hwang, Eunho Yang, and Jinwoo Shin. *RetCL: A Selection-Based Approach for Retrosynthesis via Contrastive Learning*. 2021. arXiv: 2105.00795. URL: <http://arxiv.org/abs/2105.00795>.

- [62] Zhongliang Guo, Stephen Wu, Mitsuru Ohno, and Ryo Yoshida. “A Bayesian Algorithm for Retrosynthesis”. In: *Journal of Chemical Information and Modeling* 60.10 (2020), pp. 4474–4486. URL: <https://doi.org/10.1021/acs.jcim.0c00320>.
- [63] Katsuhiko Ishiguro, Kazuya Ujihara, R. Sawada, Hirotaka Akita, and Masaaki Kotera. “Data Transfer Approaches to Improve Seq-to-Seq Retrosynthesis”. In: *ArXiv* (2020).
- [64] Haris Hasic and Takashi Ishida. “Single-Step Retrosynthesis Prediction Based on the Identification of Potential Disconnection Sites Using Molecular Substructure Fingerprints”. In: *Journal of Chemical Information and Modeling* 61.2 (2021), pp. 641–652. URL: <https://doi.org/10.1021/acs.jcim.0c01100>.
- [65] Umit V. Ucak, Taek Kang, Junsu Ko, and Juyong Lee. “Substructure-based neural machine translation for retrosynthetic prediction”. In: *Journal of Cheminformatics* 13.1 (2021), p. 4. ISSN: 1758-2946. DOI: 10.1186/s13321-020-00482-z. URL: <https://doi.org/10.1186/s13321-020-00482-z>.
- [66] Binghong Chen, Chengtao Li, Hanjun Dai, and Le Song. *Retro*: Learning Retrosynthetic Planning with Neural Guided A* Search*. 2020. arXiv: 2006.15820. URL: <http://arxiv.org/abs/2006.15820>.
- [67] John Bradshaw, Brooks Paige, Matt J Kusner, Marwin HS Segler, and José Miguel Hernández-Lobato. “A Model to Search for Synthesizable Molecules”. In: (2019). arXiv: 1906.05221. URL: <http://arxiv.org/abs/1906.05221>.
- [68] Sai Krishna Gottipati et al. *Learning To Navigate The Synthetically Accessible Chemical Space Using Reinforcement Learning*. 2020. arXiv: 2004.12485. URL: <http://arxiv.org/abs/2004.12485>.
- [69] Julien Horwood and Emmanuel Noutahi. “Molecular Design in Synthetically Accessible Chemical Space via Deep Reinforcement Learning”. In: *ACS Omega* 5.51 (2020), pp. 32984–32994. URL: <https://doi.org/10.1021/acsomega.0c04153>.
- [70] Philipp Renz, Dries Van Rompaey, Jörg Kurt Wegner, Sepp Hochreiter, and Günter Klambauer. “On Failure Modes in Molecule Generation and Optimization”. In: *Drug Discovery Today: Technologies* 32-33 (2019), pp. 55–63. URL: <https://doi.org/10.1016/j.ddtec.2020.09.003>.
- [71] H. L. Morgan. “The Generation of a Unique Machine Description for Chemical Structures-A Technique Developed at Chemical Abstracts Service.” In: *Journal of Chemical Documentation* 5.2 (1965), pp. 107–113. URL: <https://doi.org/10.1021/c160017a018>.
- [72] Aaron van den Oord, Yazhe Li, and Oriol Vinyals. *Representation Learning with Contrastive Predictive Coding*. 2018. arXiv: 1807.03748. URL: <http://arxiv.org/abs/1807.03748>.
- [73] Nadine Schneider, Daniel M. Lowe, Roger A. Sayle, and Gregory A. Landrum. “Development of a Novel Fingerprint for Chemical Reactions and Its Application to Large-Scale Reaction Classification and Similarity”. In: *Journal of Chemical Information and Modeling* 55.1 (2015), pp. 39–53. URL: <https://doi.org/10.1021/ci5006614>.
- [74] Günter Klambauer, Thomas Unterthiner, Andreas Mayr, and Sepp Hochreiter. *Self-Normalizing Neural Networks*. 2017. arXiv: 1706.02515. URL: <https://arxiv.org/abs/1706.02515>.

APPENDIX

Contents

1	Introduction	1
2	Background: single-step retrosynthesis	3
3	Modern Hopfield networks for reaction template prediction	4
4	Experiments	6
4.1	Template relevance prediction: USPTO-sm and USPTO-lg	6
4.2	Single-step retrosynthesis: USPTO-50k	8
5	Discussion and conclusion	9
A1	Notation	16
A2	Further related work	17
A3	Details on Experiments	17
A3.1	Template relevance prediction	17
A3.1.1	Datasets and preprocessing	17
A3.1.2	Data splits.	17
A3.1.3	Feature extraction.	18
A3.1.4	Training	18
A3.1.5	Hyperparameter selection and model architecture	18
A3.2	Single-step retrosynthesis	18
A3.2.1	Datasets and preprocessing	18
A3.2.2	Feature extraction	19
A3.2.3	Hyperparameters and model architecture	20
A3.2.4	Methods omitted from comparison	20
A3.2.5	Inference speed	21
A4	Additional Results	22
A5	Hopfield Association Space	24
A6	Objective and loss functions	25

A1 Notation

Definition	Symbol/Notation	Dimension
set of reaction templates	\mathcal{T}	set of size K
encoded set of reaction template	\mathbf{T}_h	$d_t \times K$
reactant molecules	\mathbf{r}	
product molecule	\mathbf{m}	
encoded molecule	\mathbf{m}_h	d_m
reaction template	\mathbf{t} or \mathbf{t}_k	
training set pair	(\mathbf{m}, \mathbf{t})	
state pattern	ξ	d
stored pattern	\mathbf{x}_k	d
stored pattern matrix	\mathbf{X}	$d \times K$
associations	\mathbf{p}	K
update function of MHN	f	
molecule encoder	\mathbf{h}^m	
reaction template encoder	\mathbf{h}^t	
model function	g	
network parameters of \mathbf{h}^m	\mathbf{w}	
network parameters of \mathbf{h}^t	\mathbf{v}	
parameters of Hopfield layer \mathbf{h}^m	$\mathbf{W}_m, \mathbf{W}_t$	$d \times \text{undef}$
association activation function	ϕ	
number of templates	K	
dimension of association space	d	

Table A1: Symbols and notations used in this paper.

In this appendix, we first provide more related work (see Section A2), then details on the experiments (see Section A3), additional results (see Section A4), visualization (see Section A5), alternative view on the loss and an extended formulation of the algorithm as pseudo-code (see Section A6).

A2 Further related work

Here we provide a broader view on works that have addressed common issues with template relevance prediction. In prior work [8, 10, 24, 26, 28, 30], template relevance prediction is often viewed as a multi-class classification task, where, given a product, an ML model is trained to predict which of the templates extracted from a reaction database are most relevant. Automatic extraction of templates leads to many rare templates, which poses a problem in the classification task as it leads to many classes with few training samples [8, 24]. In earlier work [8], rare templates were excluded from training. Baylon et al. [28] proposed a hierarchical grouping of reaction templates and trained a separate NN for each group of templates. Fortunato et al. [24] pretrained their template scoring model to predict which templates are applicable and observed that it improves template-relevance predictions, especially for rare templates. [30] used a graph-NN to predict the relevant templates. Bjerrum et al. [26] trained two separate NNs. The first NN is trained on the applicability matrix and serves for pre-filtering reaction templates. The second is trained on the reaction dataset, and ranks the reaction templates according to their relevance. Dai et al. [27] make use of the template structures. However, they factorize the predicted probabilities into multiple functions, which might not be suited to the problem. The in-scope filter of the CASP system by Segler et al. [8] also make use of template structure. Sun et al. [53] apply all templates and uses a model to rank the resulting reactants, which achieves the best top-1 accuracy but is computationally costly (Dual-TB in Table 2).

A3 Details on Experiments

A3.1 Template relevance prediction

A3.1.1 Datasets and preprocessing

For preprocessing USPTO-sm and USPTO-lg, we followed the implementation of Fortunato et al. [24]. The templates were extracted from the mapped reactions using RDChiral [49] and subsequently filtered according to symmetry, validity, and by checking if the application of the template yielded the result as in the reaction the template originated from. Despite adhering to the original implementation by the authors, our preprocessing resulted in different dataset sizes. The roughly 2 million starting reactions decreased to 443,763 samples and 236,053 reaction templates for USPTO-lg (compared to 669,683 samples and 186,822 reaction templates in Fortunato et al. [24]), and to 40,257 samples and 9,162 reaction templates for USPTO-sm (compared to 32,099 samples and 7,765 reaction templates in Fortunato et al. [24]). It can be seen that 17% of samples occur in a class that has only one sample in USPTO-sm and 43% in USPTO-lg. 66% of reaction templates in USPTO-sm and 80% in USPTO-lg occur only in a single reaction.

To allow for pretraining of the methods, we calculated the applicability matrix, i.e., which templates in a dataset are applicable to which molecules. Fortunato et al. [24] reported that this would take ~ 36 CPU-hours for USPTO-sm and ~ 330 CPU-days for USPTO-lg on a single core of a Xeon(R) Gold 6154 CPU@3 GHz. We found that using a substructure screen could speed up this procedure. The following values were obtained using an AMD EPYC 7542. For USPTO-sm it only takes us 3.3 CPU-minutes to achieve the same result. Using 16 CPU-cores this reduces to $\sim 14s$. Using 32 CPU-cores applicability calculation time for USPTO-lg reduces to $\sim 50m$ which corresponds to 27 CPU-hours compared to ~ 8000 CPU-hours for the original implementation. These comparisons should be taken with a grain of salt because of the slightly different dataset sizes and hardware used. For USPTO-lg $443\,763 \cdot 236\,053 \sim 10^{11}$ pairs have to be checked, and our code relies on a python loop. Using a compiled language could probably further speed up the procedure.

A3.1.2 Data splits.

We split the data into a training, validation, and test set following Fortunato et al. [24]. Here, a stratified split was used to ensure that templates are more equally represented across the splits. Concretely, in Fortunato et al. [24], the split proportions were 80/10/10% except for templates with

fewer than 10 samples, where one random sample was put into the test set, one into the validation set, and the rest into the training set. If only two samples were present, one was put into the test and one into the training set. Finally, if only a single sample was available for a template, it was randomly placed into the train/validation/test set with an 80/10/10% chance.

A3.1.3 Feature extraction.

Molecule fingerprints. The source molecules are represented as SMILES. We extract a fingerprint representation of the molecules. We tried out different fingerprint types, e.g. folded Morgan fingerprints with chirality [71] and the hyperparameter selection procedure (see Table A2) selected Morgan fingerprint with radius of 2 folded to 4096 features.

Template fingerprints. For the template representation, a similar procedure has been applied. A template consists of multiple enumerated SMARTS-strings. The fingerprint type for the templates was set to 'rdk'-fingerprint or 'pattern'-fingerprint for template relevance prediction and calculated for each molecule that the pattern represents. We experimented with multiple ways of combining not just the product side, but also the reactant side to this representation. We found the following to perform best among the considered variants. The fingerprints were calculated for each molecular pattern, and a disjunction over reactants as well as products was calculated. The product minus half of the reactant side results in the template fingerprint as input for the template encoder. We also tried the 'structuralFingerprintForReaction' function provided by RDKit, which concatenates the disjunction of each side of the reaction, but found the weighted combination to perform better. The resulting representation was similar and for some equal, and therefore, we added an additional random template embedding. The random noise was added to the representation of frequent templates in order to help to discriminate frequent templates with a high fingerprint similarity. Templates are classified as "frequent" if they appear at least a certain number of times in the training-set, which is determined by the hyperparameter "random template threshold" (see Table A2).

A3.1.4 Training

All models were trained for a maximum of 100 epochs on a Titan V with 12 GB RAM or a P40 with 24 GB RAM using PyTorch 1.6.0 [52]. In the case of DNN, only the molecule encoder was trained, and a linear layer, projecting from the last hidden layer to the number of templates was added. For pretraining on the applicability task we changed the loss function to the mean of binary cross-entropy for each output (template). We also experimented with InfoNCE-loss [72] on representations in Hopfield space (see Appendix A6). Because of fast convergence and slightly better performance, and because for the USPTO data sets only a single template is correct for each molecule, we use our proposed loss, which in this case is equivalent to CE-loss.

A3.1.5 Hyperparameter selection and model architecture

Hyperparameters were explored via automatic Bayesian optimization for USPTO-sm, as well as manual hyperparameter-tuning. In the former, early stopping was employed. The range of values was selected based on prior knowledge. Additional manual hyperparameter-tuning resulted in better predictive performance on the validation set. Some of the important hyperparameters are the beta scaling factor of the Hopfield layer β , the dimension of the association space d , as well as the association-activation function, or if the association space should be normalized via layer-norm [43]. An overview of considered and selected hyperparameters is given in Tab. A2. All models were trained if applicable for a maximum of 100 epochs using AdamW[46] (betas=(0.9, 0.999), eps=1e-8, weight_decay=1e-2, amsgrad=False). Hyperparameters were selected based on the minimal CE-loss on the validation set.

A3.2 Single-step retrosynthesis

A3.2.1 Datasets and preprocessing

For single-step retrosynthesis, we used the preprocessed version and splitting-procedure from Coley et al. [29]. The dataset originated from USPTO-50k by Schneider et al. [73]. It is different in details from USPTO-sm and does not contain a filtering step, whereby samples are excluded if extracted and applied templates don't yield the reactants. A further difference is the split. For USPTO-50k,

Hyperparam	Values	MHN selected (Sm/Lg)	DNN selected (Sm/Lg)
learning rates	{1e-4, 2e-4, 5e-4, 1e-3}	5e-4 / 1e-4	5e-4 / 2e-4
batch-size	{32, 128, 256, 1024}	1024	256 / 1024
dropout	[0.0, 0.6]	0.2	0.15
<i>molecule encoder</i>			
fingerprint type	{morgan, rdk}	morgan	morgan
fingerprint size	{1024, 2048, 4096}	4096	4096
number of layers	{0, 1, 2}	0	1
layer-dimension	{1024, 2048, 4096}	-	2048
activation-function	{None, SELU, ReLU}	None	ReLU
<i>template encoder</i>			
number of layers	{0, 1, 2}	0	
template fingerprint type	{pattern, rdk}	rdk	
random template thresh.	-1, 2, 5, 10, 50	2	
<i>Hopfield layer</i>			
beta	[0.01, 0.3]	0.03	
association af	{None, SELU, GeLU, Tanh}	None / Tanh	
normalize pattern	{False, True}	False	
normalize projection	{False, True}	True	
learnable stored-pattern	{False, True}	False	
hopf-num-layers	{1, 2, 3}	1	
hopf-num-Wm	{1, 2, 3}	1	
hopf-num-Wt	{1, 2, 3}	1	
hopf-FF-activation	{None, SELU, ReLU}	None	
association-dimension d	{32, 64, 512, 1024}	1024	
hopf-num-heads	{1, 6, 12}	1	
<i>Setting-specific-hps</i>			
pretraining epochs	{0,5,10,15,20,25}	10	25 / 5

Table A2: Hyperparameter search-space for template relevance prediction. The rows are subdivided into five modules: overall parameters, the molecule encoder, the template encoder, the Hopfield layer, and setting specific hyperparameters that were only used if explicitly stated. The column values show the range of the explored parameters. If multiple Hopfield layers were used, the same hyperparameters were used for all layers. A "random template threshold" of -1 corresponds to not adding noise. The fingerprint size for the molecule encoder was always the same as the template encoder. The pretraining learning rate was also defined by the learning rate, the optimizer remained the same, but the loss-function changed to binary-cross-entropy loss.

we shuffle the samples and further split it according to the procedure by Coley et al. [29], randomly splitting within the reaction types, to obtain 40008 train- 5001 validation- and 5007 test-samples (80/10/10). We computed the reaction templates only from the train- and validation-set.

A3.2.2 Feature extraction

For this experiment, we additionally explored Mixed-Fingerprint (MxFP), which is a mixture of multiple unfolded, counted (where applicable) RDKit fingerprints: MACCS, Morgan, ErG, AtomPair, TopologicalTorsion, and RDK. For each fingerprint type, we sort the features by their variance of binary fingerprints in the train-set and discard low-variance features up to a certain length. We additionally scale the counts by $\log(1 + x)$ [8].

Template-representation. We compute fingerprints for each subgraph-pattern in the reaction template. Again we use a mixture of multiple unfolded RDKit fingerprints. For pooling the reactant fingerprints, we additionally experimented with different pooling operations. The main idea is to avoid that different sets are identical after pooling and thus to increase the expressivity of the pooling operation.

Lgamma pooling is a novel pooling operation that uses the log of the gamma-function.

$$\text{lgp}(x) = \log \left(\Gamma \left(\sum_{i=0}^n x_i + 2 \right) \right) - \sum_{i=0}^n \log(\Gamma(x_i + 1)), \quad (5)$$

where the x contains a single feature of the elements of the set that is pooled. The use of this pooling function provided a small performance increase over max-pooling.

A3.2.3 Hyperparameters and model architecture

Hyperparameters were tuned manually and selected based on top-1 accuracy on the validation set. The explored parameters, as well as the selected hyperparameters, can be found in Table A3. Models were also trained if applicable for a maximum of 100 epochs using AdamW [46] (betas=(0.9,0.999), eps=1e-8, weight_decay=1e-2, amsgrad=False). As input, MxFP was selected with a fingerprint size of 30k. It consists of two layers, where the input for the second layer is $\xi^{\text{new}} + \xi$, a skip connection from the first layers input plus the output of the first layer. The first layers' memory is comprised of MxFP-template fingerprints with lgamma-pooled reactants (see Section A3.2.2). The second layer uses a different template representation: RDK-template fingerprint with additional random noise for all templates which appear more than once in the training set. The final prediction is computed by a weighted average of the individual layers' p .

The NeuralSym baseline was trained as follows: As a model architecture, we used a feed-forward neural network with a single hidden layer of size 4096 and SELU activation function [74]. The inputs to this network were ECFP-fingerprints [42] with radius 2 and size 4096. The model was trained using AdamW [46] with learning rate 1e-3 and weight-decay of 1e-3. The model was trained for 7 epochs with a batch size of 512.

A3.2.4 Methods omitted from comparison

We omitted some studies from the comparison in Table 2, despite them reporting performance on USPTO-50k. We found that the experimental settings or reported metrics in these studies differed from ours. While these reported values are not per se flawed, we think that inclusion in the comparison may be misleading. We list specifics below:

- Yan et al. [60] reported (<https://github.com/uta-smile/RetroXpert>) that their model used information in the atom-mappings about where the reaction center is. This information relies on the knowledge of the reactants. As the reactants are to be predicted in this task this is considered test set leakage.
- The reported values in [23] are also based on unintentional use of information about the reaction center, similar to above².
- The method proposed in [61] selects reactants from a candidate set. Since this candidate set is a superset of the reactants in the USPTO-50k, it might contain information about the test data. Indeed we found that we could augment the performance of our method by a process of elimination, i.e., discarding reactant sets from the predictions if they are not in the candidate set.
- The method proposed in [64] also relies on a candidate set that we suspect to contain information about the test set. However, the description of the method is not very detailed.
- Guo et al. [62] use reactants from USPTO-stereo as described in [13] as a candidate set. We found that, given this set, we could augment the performance of our method by removing reactant sets not in this set from our predictions.
- Ishiguro et al. [63] propose a pretraining step on a larger data set which does not conform to the setting in most prior work and is therefor excluded.
- Ishida et al. [30] use a different subset of USPTO-50k to train their model and report different metrics.
- Ucak et al. [65] also make use of a different subset and also do not report reactant top-k accuracy.

²Personal communication with the authors

Hyperparam	Values	MHN (50k)	DNN (50k)
learning rates	{1e-4, 2e-4, 5e-4, 1e-3}	5e-4 / 1e-4	1e-4
batch-size	{32, 128, 256, 1024}	1024	256
dropout	[0.0, 0.6]	0.2	0.15
<i>molecule encoder</i>			
fingerprint type	{morgan, rdk, MxFP}	MxFP	morgan
fingerprint size	{4096, ..., 40e3}	3e4	4096
fingerprint radius	{2, ..., 6}	-	2
number of layers	{0, 1, 2}	0	1
layer-dimension	{1024, 2048, 4096}	-	4096
activation-function (af)	{None, SELU, ReLU}	None	SELU
<i>template encoder 1</i>			
number of layers	{0, 1, 2}	0	
template fingerprint type	{rdk, rdkc, MxFP}	MxFP	
random template threshold	-1, 2, 5, 10, 50	-1	
reactant pooling	{max, sum, mean, lgamma}	lgamma	
<i>template encoder 2</i>			
number of layers	{0, 1, 2}	0	
template fingerprint type	{rdk, MxFP}	rdk	
random template threshold	-1, 2, 5, 10, 50	2	
<i>Hopfield layer 1 and 2</i>			
beta	[0.01, 0.3]	0.03	
association af	{None, Tanh}	None	
normalize input pattern	{False, True}	True	
normalize association proj.	{False, True}	True	
learnable stored-pattern	{False}	False	
hopf-num-layers	{1, 2}	2	
hopf-num-Wm	{1, 2}	1	
hopf-num-Wt	{1, 2}	1	
hopf-FF-af	{None, SELU, ReLU}	None	
association-dimension d	{32, 64, 512, 1024}	1024	
hopf-num-heads	{1, 6, 12}	1	

Table A3: Hyperparameter search-space for single-step retrosynthesis. The layout and specifics are equivalent to Table A2 but differ in the explored values and architectural choices. The hyperparameters for the Hopfield layer remain the same among layers, with individually initialized weight parameters. The input for layer 1 is given by "template encoder 1" and vice versa for layer 2. The column MHN (50k) corresponds to the results of MHNreact and DNN (50k) to the first mention of NeuralSym in Table 2.

- Liu et al. [16] only provide results for the special case where the type of reaction is provided to the model.

A3.2.5 Inference speed

We investigated the speed/performance trade-off for multiple methods. Firstly, we trained a Transformer baseline using the code and settings provided by [13], except for setting the batch size to 8192, warmup steps to 6k, and train steps to 50k. We evaluated the predictions of this model when run with beam sizes {1, 3, 5, 10, 20, 50, 75, 100}. While performance increases with larger beam size, the model also gets slower. This model outperforms the model suggested in [17], but could not reach the performance of [18]. Model training took about six hours on an Nvidia V100.

For MHN and NeuralSym, the inference procedure contains the following steps. First fingerprints for the given products have are generated. Then the model is used to predict template relevance. For each product templates are executed in the order of their score until a fixed number of reactant sets are obtained. To optimize top-k accuracy, it does not help to generate more than k reactant sets. Therefore we set the number of reactant sets to generate to {1, 3, 5, 10, 20, 50} optimize speed without loss of top-k accuracy for the respective k and measured inference time. Speeds for the Transformer,

NeuralSym, and MHN models have been measured using an Nvidia Tesla T4 and 16 cores of an AMD EPYC 7542. We also tested stopping template execution based on the cumulative probability of already executed ones as done in [8], however found that it did not improve upon stopping after a certain number of reactants have been retrieved.

A4 Additional Results

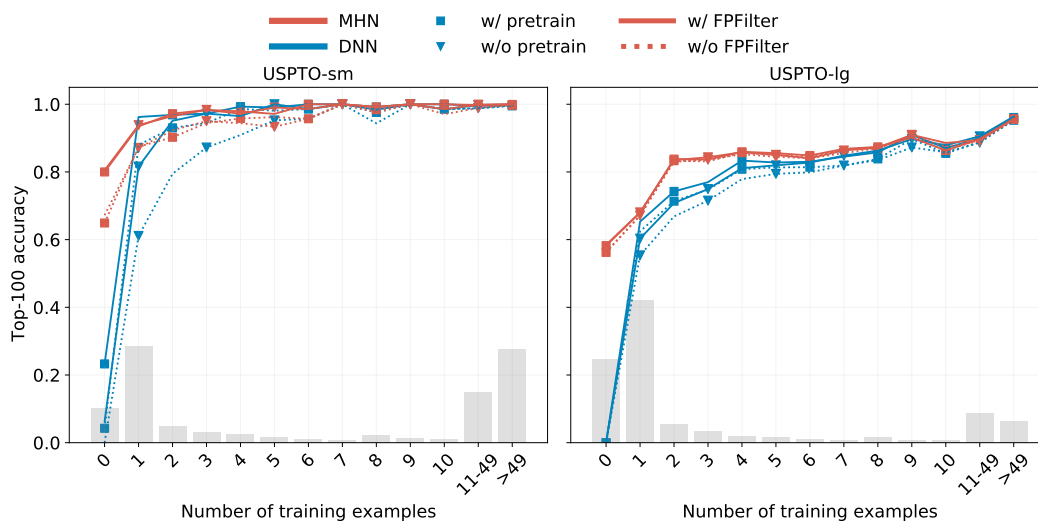


Figure A1: Results of methods with different design elements on the USPTO-sm and USPTO-lg datasets. Each method consists of a combination of the following elements: a) a network MHN or DNN (blue or red line), b) whether pretraining is applied (squares or triangles), and c) whether fingerprint filter is applied for postprocessing (solid or dashed line). These eight possible combinations are displayed as lines with their top-100 accuracy on the y-axis and the different template frequency categories on the x-axis.

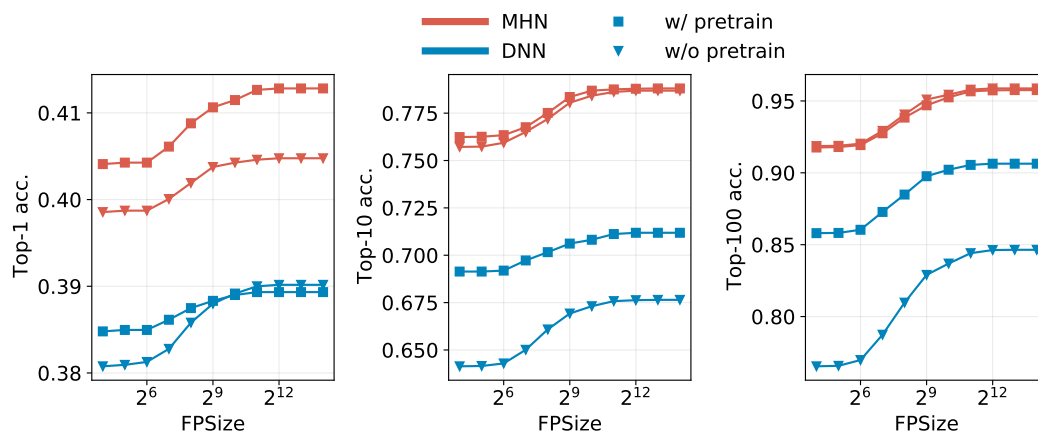


Figure A2: Predictive performance of different methods in dependency of the fingerprint size. Each method consists of a combination of the following elements: a) a network MHN or DNN (blue or red line), and b) whether pretraining is applied (squares or triangles). These four possible combinations are displayed as lines with their top-1, top-10 and top-100 accuracy. Performance saturates at a fingerprint size of about $2^{12}=4096$, and we therefore choose this value for the other experiments.

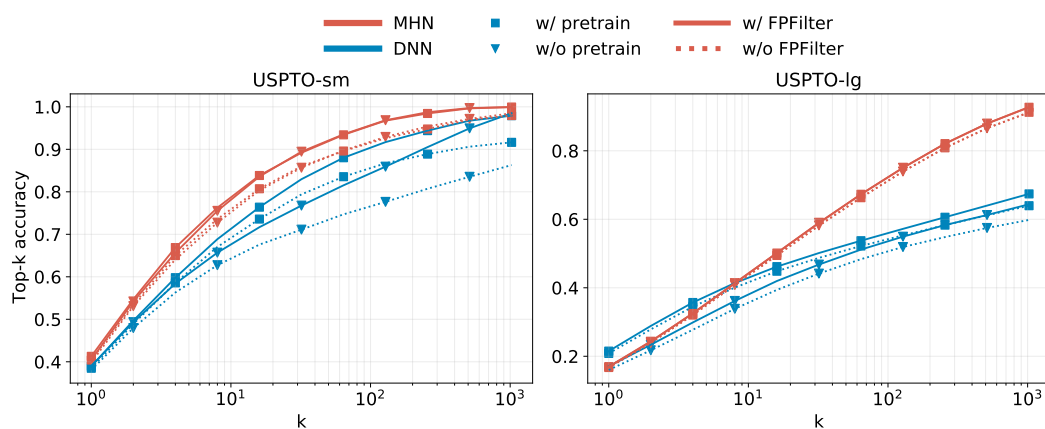


Figure A3: Comparison of methods with respect to their top-k accuracies. Each method consists of a combination of the following elements: a) a network MHN or DNN (blue or red line), b) whether pretraining is applied (squares or triangles), and c) whether fingerprint filter is applied for postprocessing (solid or dashed line). These eight possible combinations are displayed as lines with their k parameter on the x-axis and their top-k accuracy on the y-axis. MHNs provide the best top-k accuracy with k larger or equal 10.

A5 Hopfield Association Space

Figure A4 shows a t-SNE embedding of both the reaction fingerprints and the learned embeddings. Each point is colored according to its class as defined in [73].

For example, reactions belonging to the type "oxidations" can be distant in the fingerprint space (pink points in the left figure), while in their learned representations are closer (pink points in right figure). Note that our model did not have access to these reaction types. It can be seen that the chosen representation for reaction templates already captures information about the relationship, and the same reaction types are represented closer after embedding it using t-SNE.

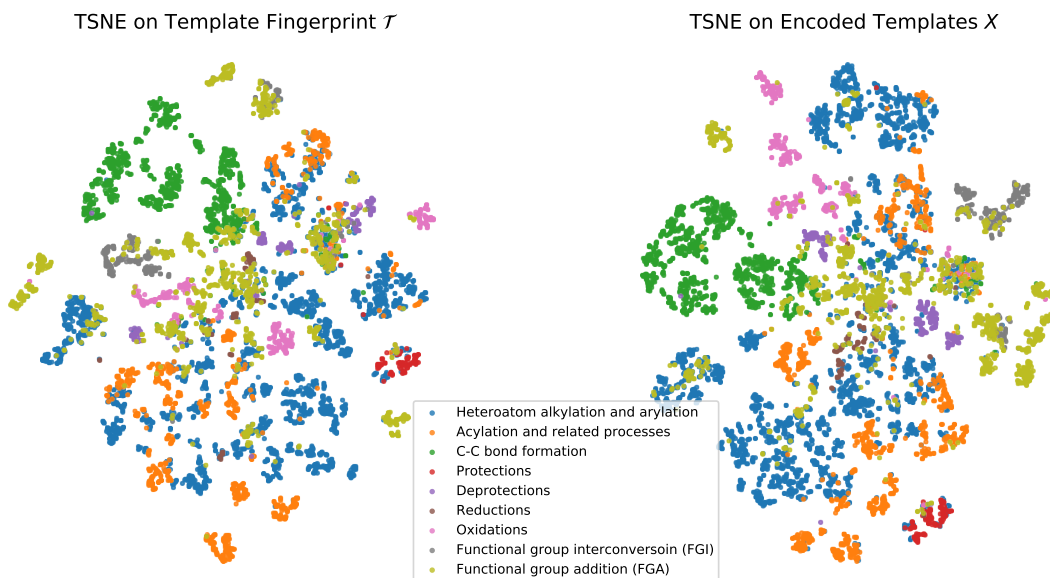


Figure A4: t-SNE downprojection of the reaction template fingerprints (left) and learned representations of reaction templates X (right). The colors represent reaction types of substructure-based expert systems as categorized by [73].

A6 Objective and loss functions

Loss on retrieved patterns. We provide a more general view on the objective and the loss function from the perspective of Hopfield networks and retrieving patterns. The main idea is to retrieve patterns from label space, rather than from Hopfield space, because the loss functions operate in the label space. The last Hopfield layer of our architecture supplies both \mathbf{p} , the softmax vector of probabilities of drawing reaction templates, and $\boldsymbol{\xi}^{\text{new}}$, an average of reaction template representations \mathbf{x} . However, averages of reaction templates are no longer reaction templates, but we are interested in the *probability* ℓ_ξ of drawing a \mathbf{x}_k that fits to $\boldsymbol{\xi}$. The probability ℓ_ξ can still be computed via a slightly modified Hopfield network update, where instead of retrieving from a memory \mathbf{X} of template representations in Hopfield space, we retrieve from the space of labels or scores. Such an update has been introduced previously and uses stored patterns that are augmented by labels [35, p.83ff].

The probability ℓ_ξ of drawing a \mathbf{x}_k that fits to $\boldsymbol{\xi}$ can be computed by a modified Hopfield network update:

$$\mathbf{q}_\xi = \mathbf{L} \mathbf{p} = \mathbf{L} \text{softmax}(\beta \mathbf{X}^T \boldsymbol{\xi}), \quad \ell_\xi = \mathbf{1}^T \mathbf{q}_\xi, \quad (6)$$

where $\mathbf{L} \in \mathbb{R}^{K \times K}$ is the diagonal matrix of labels that are zero or one and $\mathbf{1} \in \mathbb{R}^K$ is the vector of ones. In general, \mathbf{L} can be used to include unlabeled data points as stored patterns, where \mathbf{L} is a Gram matrix times a diagonal label matrix to transfer label information from labeled data points to unlabeled data points. $L_{kk} = 1$ means that \mathbf{x}_k fits to $\boldsymbol{\xi}$ and $L_{kk} = 0$ means that \mathbf{x}_k does not fit to $\boldsymbol{\xi}$. In the context of the Hopfield networks, if more than one \mathbf{x}_k fits to $\boldsymbol{\xi}$ then all \mathbf{x}_k that fit to $\boldsymbol{\xi}$ constitute a metastable state. Instead of L_{kk} being equal to zero or one, L_{kk} can give a non-negative score for how well \mathbf{x}_k does fit to $\boldsymbol{\xi}$. In this case ℓ_ξ is the *expected score*.

In this general view, our objective is to minimize $-\log(\ell_\xi)$. If L_{kk} is equal to zero or one, $\log(\ell_\xi)$ is the log-likelihood of drawing a fitting \mathbf{x}_k . If only one \mathbf{x}_k fits (exactly one L_{kk} is one), then our objective is equivalent to the cross-entropy (CE) loss for multi-class classification. However, if more \mathbf{x}_l are labeled as fitting, then our objective is different from CE, which might not be appropriate. If L_{kk} is a non-negative score for the molecule-template pair, our approach will maximize the expected score.

Cross-entropy loss. In a simple setting, in which each molecule only has a single correct reaction template in \mathcal{T} , a categorical cross-entropy loss is equivalent to the suggested loss. We encode the correct template by a one-hot vector $\mathbf{y} = (0, \dots, 0, 1, 0, \dots, 0)$, where 1 indicates the position of the correct template in the template set $\mathcal{t} = \mathcal{t}^k$. We then minimize the cross-entropy loss function $\ell_{\text{CE}}(\mathbf{y}, \mathbf{p}) = \text{crossentropy}(\mathbf{y}, \mathbf{p})$ between ground truth \mathbf{y} and the model’s predictions \mathbf{p} for a single pair of the training set and the overall loss is an average over all such pairs. The corresponding algorithm is given in Alg. 2.

InfoNCE in Hopfield space. An almost equivalent loss function would be to use a contrastive loss on the retrieved pattern $\boldsymbol{\xi}^{\text{new}}$. This contrastive loss measures the cosine similarity of the retrieved pattern with the correct stored patterns with the InfoNCE function [33, 72]:

$$\ell_p(\boldsymbol{\xi}^{\text{new}}, \mathbf{x}^+, \mathbf{X}^-) = \text{InfoNCE}(\boldsymbol{\xi}^{\text{new}}, \mathbf{x}^+, \mathbf{X}^-) = -\log \frac{\exp(\text{sim}(\boldsymbol{\xi}^{\text{new}}, \mathbf{x}^+)/\tau)}{\sum_k \exp(\text{sim}(\boldsymbol{\xi}^{\text{new}}, \mathbf{x}_k^-)/\tau)}, \quad (7)$$

where $\text{sim}(\cdot, \cdot)$ is a pairwise similarity function, \mathbf{x}^+ is the representation of the correct reaction templates, and \mathbf{X}^- is the set of representations of the incorrect reaction templates, that are contrasted against each other. This loss is equivalent to cross-entropy loss if a) the denominator of Eq. (7) would use all pairs and not only negative pairs (this variant is a frequently used version of InfoNCE), b) $1/\tau = \beta$, c) the similarity function is the dot product, and d) $\boldsymbol{\xi}$ is used instead of $\boldsymbol{\xi}^{\text{new}}$. Our experiments show that the pattern loss can lead to models with comparable performance to those trained with cross-entropy loss. The according algorithm with pattern loss as alternative loss is shown in Alg. 2.

We provide a formulation of our method as simplified pseudo-code in a Python/Pytorch[52]-like language (see Algorithm 2). The pseudo-code provides a version with two stacked Hopfield layers and three possible formulations of the loss function.

Algorithm 2 MHN for reaction template prediction (simplified, e.g. skip-connections omitted).

```
# mol_encoder() — e.g. fully-connected or MPNN. Maps to dimension  $d_m$ .
# template_encoder1() Maps to dimension  $d_{t_1}$ .
# template_encoder2() Maps to dimension  $d_{t_2}$ .
# m_train, t_train — pair of product molecule and reaction template from training set
# T — set of  $K$  reaction templates including t_train
# d — dimension of Hopfield space

## FORWARD PASS
T1_h = template_encoder1(T)#[d_t1,K]
T2_h = template_encoder2(T)#[d_t2,K]
m_h = mol_encoder(m_train)#[d_m,1]
xinew1,_,_ = Hopfield(m_h,T1_h,dim=d)
xinew,p,X = Hopfield(xinew1,T2_h,dim=d)
p=pool(p,axis=1) #[K,1]

## LOSS
# association loss
label = where(T==t_train)#[K,1]
loss = cross_entropy(p,label)
# alternative 1: Hopfield loss
L = diag(where(T==t_train))#[K,K]
loss = -log(sum(L@p))
# alternative 2: pattern loss
label = where(T==t_train)#[K,1]
pos = X[label] #[d,1]
neg_label = where(T!=t_train)#[K,1]
neg = X[neg_label] #[d,K-1]
loss = -InfoNCE(xinew,pos,neg)
```
